PNAS RESEARCH ARTICLE | EVOLUTION

Phylogenomics of the psychoactive mushroom genus *Psilocybe* and evolution of the psilocybin biosynthetic gene cluster

Alexander J. Bradshaw[a,b,1,2], Virginia Ramírez-Cruz[c,1], Ali R. Awan[d], Giuliana Furci[e], Laura Guzmán-Dávalos[f], and Bryn T. M. Dentinger[a,b,2]

Edited by Pamela Soltis, University of Florida, Gainesville, FL; received July 20, 2023; accepted November 28, 2023

Psychoactive mushrooms in the genus *Psilocybe* have immense cultural value and have been used for centuries in Mesoamerica. Despite the recent surge of interest in these mushrooms due to the psychotherapeutic potential of their natural alkaloid psilocybin, their phylogeny and taxonomy remain substantially incomplete. Moreover, the recent elucidation of the psilocybin biosynthetic gene cluster is known for only five of ~165 species of *Psilocybe*, four of which belong to only one of two major clades. We set out to improve the phylogeny of *Psilocybe* using shotgun sequencing of fungarium specimens, from which we obtained 71 metagenomes including from 23 types, and conducting phylogenomic analysis of 2,983 single-copy gene families to generate a fully supported phylogeny. Molecular clock analysis suggests the stem lineage of *Psilocybe* arose ~67 mya and diversified ~56 mya. We also show that psilocybin biosynthesis first arose in *Psilocybe*, with 4 to 5 possible horizontal transfers to other mushrooms between 40 and 9 mya. Moreover, predicted orthologs of the psilocybin biosynthetic genes revealed two distinct gene orders within the biosynthetic gene cluster that corresponds to a deep split within the genus, possibly a signature of two independent acquisitions of the cluster within *Psilocybe*.

phylogenomics | psychoactive | mushroom | *Psilocybe* | evolution

Significance

Therapeutic use of psilocybin from "magic mushrooms" is revolutionizing mental health treatment for many conditions, including depression, PTSD, and end-of-life care. However, knowledge of *Psilocybe* diversity and its evolutionary history is substantially incomplete. Our study presents the most extensive phylogenomic dataset across *Psilocybe* to date, with 23 samples derived from type specimens. Using ~3,000 single-copy gene families, we recovered a robust and well-supported phylogeny. Mapping psilocybin biosynthetic gene orthologs on the phylogeny revealed two types of gene cluster order corresponding to a deep split in the genus. Molecular dating suggests psilocybin biosynthesis arose in *Psilocybe* ~67 mya, concurrent with the K-Pg mass extinction event. A significant advancement in the understanding of *Psilocybe* evolution and psilocybin biosynthesis is presented.

Psilocybin, the psychoactive natural product found in some mushrooms and other *Fungi*, is at the forefront of a wave of recent research showing the tremendous potential of psychedelic drugs for a wide range of mental health therapies and understanding human consciousness (1–3). Although species of *Psilocybe* (Fr.) P. Kumm. (first described as *Agaricus semilanceatus* Fr.) have been known to the scientific community since the early 19th century (4), *Psilocybe* mushrooms have been used across Mesoamerica for centuries, particularly in spiritual ceremonies (5–13). In many of these indigenous cultures, their use is considered sacramental or devoted to healing practices. It was for this reason that with the arrival of European colonialism, in most cases, these cultures experienced religious persecution for their use of these mushrooms (5). This renewed interest in psilocybin has shined a spotlight on the organisms that produce them, most of which belong to a single genus of mushroom, *Psilocybe*. Colloquially known as "magic mushrooms," their psychoactive properties were made widely known in 1957 when Robert Gordon Wasson published his personal experiences with them in *Life* magazine (14). However, since Nixon's 1971 "war on drugs" campaign in the United States, psilocybin and its analogs have been listed on Schedule 1 of the Controlled Substances Act, making possession of the compounds without a special license a federal crime. This legal status stifled research on psilocybin and the organisms that produce it for the last 50+ years (11).

New research in the last six years has yielded surprising insights into the biosynthesis and evolution of psilocybin. In most *Fungi*, psilocybin is synthesized by four core enzymes [PsiD (tryptophan decarboxylase), PsiK (kinase), PsiM (methyltransferase), and PsiH (P_{450} monooxegynase)] that convert the amino acid tryptophan into psilocybin and whose genes occur in a biosynthetic gene cluster (BGC) (15). BGCs constitute close proximity clustering of genes related to the biosynthesis of secondary metabolites, which are commonly used for accessory metabolic functions such as chemical defense or metabolism of variable carbon sources (16). The close proximity allows for efficient and coordinated expression of the genes in the cluster, which often serve complementary functions in the production of a specific secondary metabolite (17). In *Fungi*, secondary metabolite production through BGCs is common in the biosynthesis of many important compounds, such as melanin and penicillin (18). However, BGCs are not strictly limited to Fungi and can be found across a wide variety of prokaryotes and eukaryotes. For example, the well-studied lactose operon ("lac operon") encodes enzymes directly related to the metabolism of lactose as a carbon source and is analogous to a BGC in that genes of the operon are tightly linked but regulated by a single promoter. Similarly, "pathogenicity islands," such as SPI-II in *Salmonella* spp., contain a multitude of genes that are expressed in a

Author contributions: A.J.B., G.F., and B.T.M.D. designed research; A.J.B., V.R.-C., and A.R.A. performed research; V.R.-C., A.R.A., L.G.-D., and B.T.M.D. contributed new reagents/analytic tools and fungal specimens; A.J.B., V.R.-C., and A.R.A. analyzed data; and A.J.B., V.R.-C., L.G.-D., and B.T.M.D. wrote the paper.

The authors declare no competing interest.

This article is a PNAS Direct Submission.

[1]A.J.B. and V.R.-C. contributed equally to this work.

[2]To whom correspondence may be addressed. Email: alexander.j.bradshaw@gmail.com or bryn.dentinger@gmail.com.

This article contains supporting information online at https://www.pnas.org/lookup/suppl/doi:10.1073/pnas.2311245121/-/DCSupplemental.

Published January 9, 2024.

coordinated and systematic manner, akin to BGC expression, and directly confer the ability to become pathogenic in numerous hosts (19, 20). In plants, BGCs are involved in chemical defenses against insect herbivory, such as in the biosynthesis of morphine and nepetalactone (21, 22). BGCs have also been found in animals, such as ancient plant-like terpene BGCs in corals that generate antifeedant chemicals (23). While secondary metabolites are not necessarily directly related to primary growth and development, they provide a system in which an organism can favorably alter interactions within its environment, making them essential to the evolutionary ecology of all life (16).

The canonical psilocybin BGC is highly conserved across the handful of species investigated (24–27) and has been reportedly acquired by mushrooms outside of *Psilocybe* through horizontal gene transfer (HGT) (25) and convergent evolution (24). However, only five of the ~165 species of *Psilocybe* (11) have been investigated at a genomic-level and only 24 have been included in multi-locus molecular phylogenetic datasets (10, 28). Thus, the tempo, mode, and timing of the evolution of the psilocybin BGC remains largely unknown, impeding our ability to construct a robust predictive framework for elucidating evolutionary patterns and the discovery of novel therapeutics.

In this study, we generated genomic-level data from 71 *Psilocybe* taxa using fungarium specimens, including 23 types. Type specimens are the ultimate authority for applying names to other collections and are therefore essential references for accurately naming and describing diversity (29). In recent years, generating DNA sequences from historical specimens ("museomics") has benefited from advances in DNA extraction methods, and the increasing accessibility and cost reduction of amplicon-independent high-throughput sequencing (30–33). Historical collections represent hundreds of years of the collective effort and serve as a significant concentration of rare and unique samples (34–36). Outside of a handful of common species, *Psilocybe* spp. are not commonly collected, and many specimens are only represented by a single collection, making research with them tremendously difficult (11).

Using the metagenomic data derived from our voucher specimens, we set out to construct a robust, time-calibrated phylogeny. We then bioinformatically mined the primary psilocybin BGC and mapped the core genes on the phylogeny to investigate the tempo, mode, and patterns of its evolution. We also investigated the timing of the origin and purported horizontal acquisition events of the psilocybin BGC by combining publicly available data from all known mushrooms with the psilocybin BGC to gain insight into the evolutionary forces that gave rise to psilocybin biosynthesis.

Results

Sequencing and Genome Assembly. Metagenomic shotgun sequencing was performed on 74 samples, including 71 identified as *Psilocybe* and three from other taxa known to produce psilocybin. These specimens were all derived from museum vouchers ranging in age from 3 to 74 y, with one sample missing a collection date (*SI Appendix*, Table S1). Total reads for samples ranged from 3,909,488 reads (Psilocybe_mexicana_IBUG-13593, ~11.7x coverage) to 225,748,454 reads (Psilocybe_baeocystis_WTU-F-011245, ~ 677.2x coverage). Across all of our samples, we achieved an average of 94,490,694 reads (~283.5x coverage) and a median of 99,070,482 reads (~297.2x coverage). Genome assembly completeness as measured by the N50 statistic ranged from N50 = 554 (Psilocybe_tuberosa_WTU-F-011378) to N50 = 60,042 (Psilocybe_stuntzii_WTU-F-011520). The number of contigs ranged from 7,004 (Psilocybe_stuntzii_WTU-F-011520) to 784,732 (Psilocybe_caerulescens_var_mazatecorum_SFSU-F-029971). BUSCO scores ranged from 30.7% (Psilocybe_fuliginosa_NY-1901148) to 95.4% (Psilocybe_stuntzii_WTU-F-011520). It should be noted that these assemblies are likely to be highly discontiguous due to low endogenous DNA content from museum specimens and should be treated as metagenome assemblies, but that are nonetheless useful for phylogenomics (37). A complete summary of sequencing results and genome assembly statistics is available in *SI Appendix*, Table S2.

***Psilocybe* Phylogenomic Analysis and Divergence Time of Major Clades.** Multiple sequence alignment statistics for the *Psilocybe*-only dataset revealed 87% (2,615) single-copy genes were recovered for all samples, 11% (339) recovered between 60 and 61 samples, and less than 1% (29) recovered fewer than 60 (*SI Appendix*). Phylogenetic analysis revealed 52/71 were true *Psilocybe* (*Psilocybe* sensu stricto) (incl. 20 types) (Fig. 1) and the other 19 were found to belong to other genera: 14 specimens correspond to *Deconica* (W.G. Sm.) P. Karst. (three types, combined in *SI Appendix*, *Results and Discussion*), three form a monophyletic group of uncertain placement within *Strophariaceae,* one corresponded to *Kuehneromyces* (Psilocybe_laticystis_UBC-F16759, sister to all of *Deconica*), and one (Psilocybe_washingtonensis_WTU-F-055019) was unable to be accurately assigned to an existing genus and was therefore removed from further analysis (*SI Appendix*, Fig. S1 and Table S1).

Phylogenetic analysis of the concatenated supermatrix and summary coalescent analysis of individual gene trees yield topologically identical phylogenies with strong support for most nodes except for two nodes internal to species clades with multiple representatives (*SI Appendix*, Figs. S1 and S2). An ancient divergence within *Psilocybe* was recovered, corresponding to Clades I & II in Ramírez-Cruz et al. (10). The phylogenetic relationships of 39 *Psilocybe* species are reported (Fig. 2, *Left*).

The stem age of *Psilocybe* was estimated at 67.61 mya with the crown age estimated at 56.43 mya (Fig. 2, *Left*; see also supplementary data on Dryad). The LTT plot does not deviate from the null hypothesis of linear growth (Fig. 2, *Left*). If a pattern of exponential growth were present instead, it would suggest that *Psilocybe* has undergone an evolutionary radiation or contraction, which is not supported by our data.

Incorporating Publicly Available Sequences. Across all publicly available sequences, 40 species were represented, ~24% of the approximately 165 currently accepted *Psilocybe* s.s. (11). However, sequence number and taxonomic representation of molecular markers varied widely. No species retrieved from the public databases had all gene regions representing a single voucher specimen. We retrieved 26 ITS, 32 Ef1a, 30 RPB1, and 32 RPB2 sequences from public databases representing 11, six, nine, and three species not represented in the genomic dataset, respectively. In total, the combined datasets were represented by 67 unique taxa, 17 of which were only available from public databases (*SI Appendix*, Figs. S3–S6).

Misidentification is a common issue in fungaria and *Psilocybe* specimens in particular (11, 29). In our study, we identified four specimens that were consistently incongruent with the other taxa they clustered with: "*Psilocybe acutissima*" (GAM00011063), "*Psilocybe baeocystis*" (WTU-F011245), "*Psilocybe quebecensis*" (NY1901130), and "*Psilocybe silvatica*" (VPI-F0003693). These specimens were reexamined microscopically and redetermined as *Psilocybe hoogshagenii* R. Heim (GAM00011063), *Psilocybe cyanescens* Wakef. (WTU-F01124), and *Psilocybe caerulipes* (Peck) Sacc. (NY1901130, VPI-F0003693) (*SI Appendix*, Table S1).

Fig. 1. Diversity of *Psilocybe* sensu stricto. (*A*) *Psilocybe azurescens* (image credit, Paul Stamets), (*B*) *Psilocybe cyanescens* (image credit Bryn T.M. Dentinger), (*C*) *Psilocybe semilanceata* (image credit Giuliana Furci), (*D*) *Psilocybe zapotecorum* (image credit Bryn T.M. Dentinger), (*E*) *Psilocybe cubensis* (image credit Oscar Castro-Jauregui), (*F*) *Psilocybe bohemica* (image credit Jan Borovička), (*G*) *Psilocybe yungensis* (image credit Virginia Ramírez-Cruz), and (*H*) *Psilocybe mexicana* (image credit Oscar Castro-Jauregui).

Identification of Psilocybin BGC Genes in *Psilocybe*. In most cases, the gene predictions from exonerate matched those from Augustus/RBB, with disagreements still having correct gene hits. In a few cases, we found that exonerate identified genes more accurately and with less ambiguity compared to our RBB method (*SI Appendix*, Table S3).

We found variability in the order of the four-core psilocybin-producing cluster genes within our expanded representation of *Psilocybe* species, identifying two distinct patterns. The first pattern followed a gene order of PsiD > PsiM > PsiH > PsiK, the canonical gene order originally reported from *Psilocybe cubensis* and *Psilocybe serbica* M. M. Moser & E. Horak, which was represented entirely

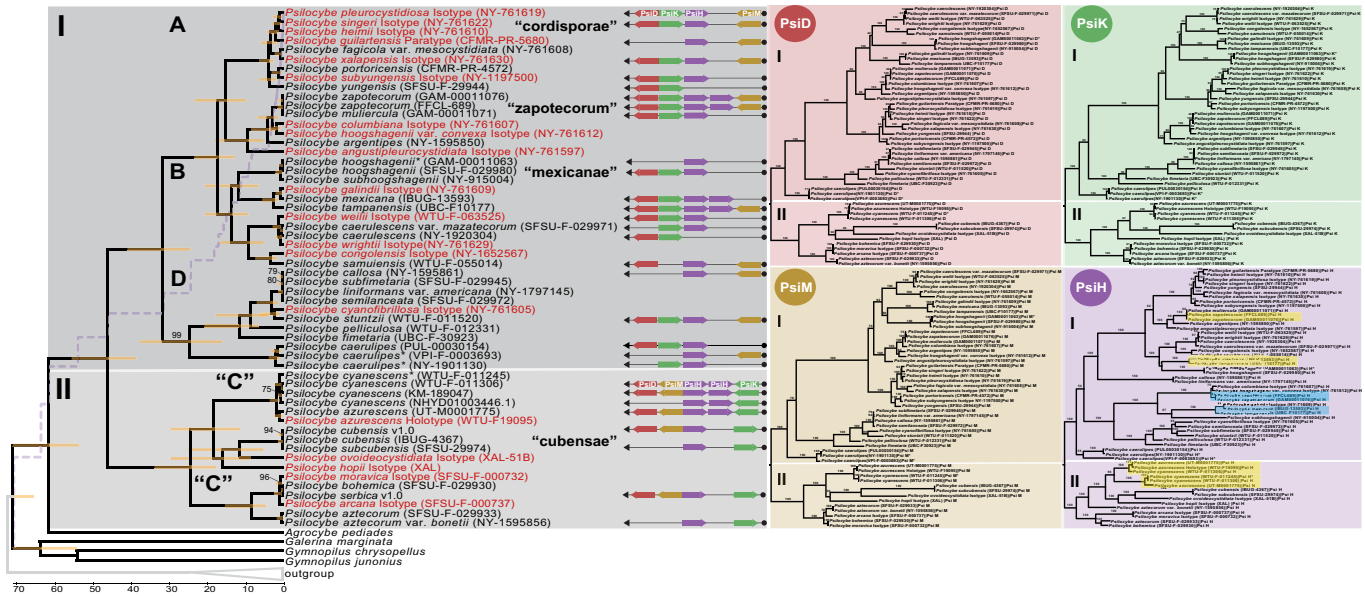

Fig. 2. *Psilocybe* phylogenomic tree and evolution of the psilocybin BCG. *Left*: Phylogenomic tree of *Psilocybe* estimated from a gene-partitioned concatenated supermatrix of 2,983 single-copy gene families estimated in IQ-TREE. Tree is rooted with an outgroup consisting of *Hebeloma cylindrosporum* and *Pholiota alnicola*. All nodes received 100% ultrafast bootstrap support in the concatenated analysis except where indicated. Topology is identical to summary coalescence of individual gene trees except for the terminal relationships within the *P. cyanescens* species cluster. Time-transformed branch lengths and divergence dates were estimated from loci with 100 clock-like, well-supported gene trees in RelTime using two internal calibrations based on the ages for Strophariaceae/Hymenogastraceae and *Gymnopilus*, reported by Varga et al. (38) and Ruiz-Dueñas et al. (39). Divergence time 95% HPD confidence bars are depicted in gold. Branch labels are percent nonparametric bootstraps implemented using the within-partition ultrafast bootstrapping option in IQ-TREE. The lineage through time plot is represented by a purple dashed line. Sequences derived from type specimens are labeled in red. The psilocybin BGC is depicted by arrows to the right of the terminal labels. Arrows are oriented according to the coding direction for each gene as determined through reciprocal best BLAST hits and color-coded by gene (PsiD = red, PsiK = green, PsiH = purple, PsiM = gold). Absence of genes indicates that placement in context of the whole cluster could not be reliably determined bioinformatically. *Right*: Maximum-likelihood phylograms for each of the four core genes from the psilocybin-producing gene cluster, PsiD (red), PsiK (green), PsiM (gold), and PsiH (purple). For enhanced readability, trees are midpoint rooted or rooted at the node leading to Clade II (PsiH). Duplicated PsiH genes are highlighted in yellow (full length) or blue (truncated). The two major clades from the organismal phylogeny are labeled with roman numerals and with shaded boxes in the background. Numbers on branches are percent nonparametric rapid bootstraps implemented using the within-partition ultrafast bootstrapping option in IQ-TREE.

by Clade II of our dataset. The second was PsiD > PsiK > PsiH > PsiM, found in Clade I of our organismal phylogeny (Fig. 2, *Right*). Across our phylogeny, the original pattern was represented by 17 *Psilocybe* specimens, while 35 of our *Psilocybe* specimens exhibited the non-canonical pattern.

In addition to gene order and orientation, we investigated the evolution of each gene separately. Phylogenetic analysis was performed without using our species constraint tree for each of the core psilocybin-producing genes, PsiD, PsiK, PsiM, and PsiH (Fig. 2, *Right*). We found that PsiD, PsiK, and PsiM were topologically congruent with the organismal phylogeny, suggesting a vertical inheritance pattern for these genes in *Psilocybe*. In contrast, PsiH was largely topologically consistent with the organismal phylogeny, but multiple taxa in both Clade I and Clade II were found to have duplicated copies of PsiH that were recovered as paraphyletic (Fig. 2, *Right*, and *SI Appendix*, Table S3). In all cases, both copies of PsiH are found in tandem on the same contig (*SI Appendix*, Table S3). One copy of PsiH in each of *P. zapotecorum*, *P. mexicana*, and *P. tampanensis* is truncated, indicating they are not functional. The phylogenetic topology of the Clade I duplications is consistent with an ancient duplication followed by gene loss in most taxa, with relict, incompletely degenerated copies persisting in only a few lineages.

Psilocybin Homologs Genes Present Outside of *Psilocybe* and Ecological Niche Patterns. We also investigated the known HGT events from *Panaeolus* (Fr.) Quél., *Gymnopilus* P. Karst., and *Pluteus* Fr., using publicly available data and specimens sequenced in this study vouchered as *Gymnopilus luteofolius* (Peck) Singer, *Pluteus albostipitatus* (Dennis) Singer, and *Pluteus salicinus* (Pers.) P. Kumm (*SI Appendix*, Table S1 and Fig. 3, *Left*). Gene prediction and RBB analysis yielded representation of the four-core psilocybin-producing genes from the published genomes of *Panaeolus cyanescens* and *Gymnopilus dilepis* (Berk. & Broome) Singer, and our *Gymnopilus luteofolius* and *Pluteus salicinus* data (*SI Appendix*, Table S1).

Phylogenetic analysis of the PsiD gene, including those from our *Psilocybe* genomic samples, and publicly available sequences, revealed three branching patterns for our non-*Psilocybe* taxa. The first branch contained *Conocybe smithii* Watling (= *Pholiotina smithii* (Watling) Enderle) as a monophyletic branch sister to our *Psilocybe caerulipes* (Peck) Sacc. samples (BS 100%). The second branch placed *Panaeolus cyanescens* as a sister group to *Psilocybe cubensis* (BS 100%), and the final contained species of both *Gymnopilus* and *Pluteus* sharing a most recent common ancestor with all of *Psilocybe* (BS 100%) (Fig. 3, *Left*).

After expanding *Psilocybe* diversity and refining the placement of known HGT events, we sought to identify whether phylogenetic clusters could be attributed to specific ecological niches. Ancestral state reconstruction was performed on the organismal phylogeny, showing a wood decay ecology as the ancestral condition in the most recent common ancestor (MRCA) of Clades I and II, with two independent specializations to coprophilic lifestyles in each (*SI Appendix*, Fig. S7). Interestingly, our two primary phylogenetic clades correspond to distinct ecological lifestyles, with a few notable exceptions (Fig. 3, *Left*). Clade I, identified through our PsiD analysis, corresponds almost entirely to the soil-dwelling saprotrophic lifestyle, except for the *Psilocybe caerulipes* cluster, which exhibits wood decay ecology (i.e., rotting wood rather than soil enriched with woody debris). *Psilocybe* Clade II, *Gymnopilus*, and *Pluteus* were associated primarily with wood decay, and in the case of *Psilocybe cubensis* and *Panaeolus cyanescens*, a coprophilous lifestyle (Fig. 3, *Left*).

Evolutionary Origins and Timing of the Psilocybin BGC in Mushrooms. Divergence dating is consistent with the earliest possible origin of the psilocybin BGC in *Psilocybe* approximately ~67 mya with subsequent acquisitions by four other genera between ~40 (*Panaeolus*) and ~9 (*Gymnopilus*) mya (Fig. 3, *Right* and *SI Appendix*). The crown age of *Psilocybe* was estimated at ~57 mya in the phylogenomic dataset, which predates the estimated origin of psilocybin in the next possible oldest lineage, *Panaeolus*. However, the relative ages of the psilocybin-producing *Panaeolus* stem and the crown age of *Psilocybe* in the LSU dataset suggest the earliest possible origin could be in *Panaeolus*. Additionally, two species of *Panaeolus* and two species of *Gymnopilus* known to contain the psilocybin BGC were paraphyletic in the LSU phylogeny. The most parsimonious interpretation is that the psilocybin BGC was gained twice independently in each genus. The first acquisition in *Panaeolus* (*Pa.*) is in *Pa. subalteatus* ~40 mya with a second acquisition ~16 mya in *Pa. cyanescens*. The first acquisition in *Gymnopilus* is in *G. aeruginosus* ~22 mya with a second in *G. junonius* ~9 mya. The psilocybin BGC was gained in *Pluteus* ~22 mya and in *Pholiotina* ~11 mya (*SI Appendix*). To further test the notion that these acquisitions were due to HGT, we performed a topological constraint test. The likelihoods of the best ML trees for PsiD from topologically constrained and unconstrained searches were −8780.501249 and −8699.391458, respectively. Tree topology test statistics universally rejected the constrained topology, corroborating the results of Reynolds et al. (25) and consistent with expectations from HGT (*SI Appendix*, Table S4).

Discussion

Phylogenomics of *Psilocybe*. Our phylogenomic analysis resulted in a single, unambiguous and statistically well-supported phylogeny for 52 specimens of *Psilocybe* s.s., resolving key nodes that were previously unsupported (Fig. 2, *Left*). Total topological congruence inferred from a partitioned supermatrix analysis and a summary coalescence of individual gene trees demonstrates that the inferred phylogeny is robust to the methodological approach and indicates low levels of gene discordance within *Psilocybe*.

The ancient divergence within *Psilocybe* first reported by Ramírez-Cruz et al. (10) was also recovered here. This early split coincides with the genic arrangement of the psilocybin BGC (Fig. 2, *Left*) but precedes a shift in ecology. Our results suggest that *Psilocybe* arose as primarily a wood-decomposing group that transitioned to soil after the split, with two independent specializations on herbivore dung (*SI Appendix*, Fig. S7). However, additional critical species, such as the African dung-dwelling *P. natalensis* Gartz, D.A. Reid, M.T. Sm. & Eicker, will need to be included to reconstruct evolution of ecologies more confidently in *Psilocybe* (further discussed in *SI Appendix*).

Origin of the Psilocybin BGC. Reynolds et al. (25) speculated that the psilocybin BGC may have originated in *Fibularhizoctonia* G.C. Adams & Kropp, a genus of anamorphic (asexually reproducing) *Athelia* Pers. that has multiple copies of Psi homologs, albeit not contained in a cluster (40). The *Atheliales* are close relatives of the *Agaricales* with a broad range of ecologies, including termite symbionts (41), plant pathogens, mycorrhizal mutualists, and saprobes. Reynolds et al. (25) speculated that this insect association may have provided the selective force for the evolution of psilocybin as a modulator of the symbiosis. Interestingly, *Athelia arachnoidea* (Berk.) Jülich is mycoparasitic on lichens common on tree bark in north temperate regions (42, 43), whereas its anamorph *Fibularhizoctonia carotae* (Rader)

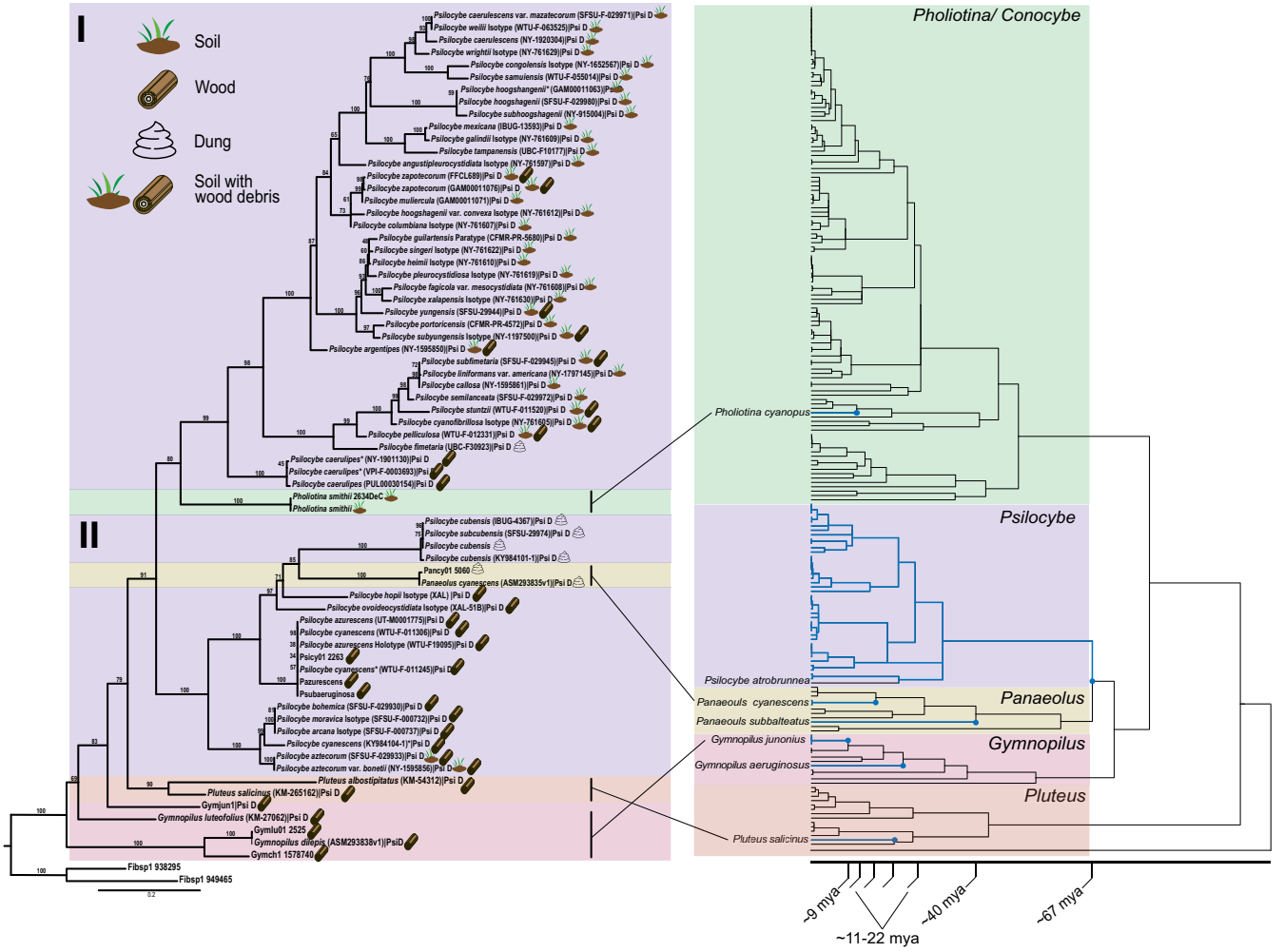

Fig. 3. PsiD gene tree and LSU gene tree of psilocybin-producing mushrooms and their inactive relatives. *Left*: Maximum-likelihood phylogram of *Agaricomycetes* PsiD homologs. Tree is rooted with *Phallomycetidae* following Reynolds et al. (25). Numbers on branches are percent nonparametric rapid bootstraps implemented using the within-partition ultrafast bootstrapping option in IQ-TREE. Icons depicting ecological niche are indicated to the *Right* of the terminal labels and legend is depicted in the *Upper left*. Major clades are denoted with roman numerals and background shading. *Right*: Maximum-likelihood time tree of all publicly available LSU sequences for species with the homologous canonical psilocybin BGC and their non-active relatives. Tree is rooted with *Calocybe gambosa* following the *Agaricales* topology in Dentinger et al. (37). Species with the psilocybin BGC are indicated by blue branches. Genera are color-coded in each tree with lines and terminal labels to corresponding psilocybin-producing taxa outside of *Psilocybe* in the PsiD tree. Nodes where the earliest possible acquisition of the psilocybin BGC likely occurred are indicated by blue dots. Time scale is at the bottom with the inferred dates of psilocybin BGC acquisition for each lineage indicated by hashmarks.

G.C. Adams & Kropp is pathogenic on carrot roots (44). Our results suggest wood decomposition as the ancestral ecology of *Psilocybe*. Both *Gymnopilus* and *Pluteus* are also wood decomposers. The mycoparasitic ecology of the teleomorphic (sexually reproducing) *Athelia arachnoidea* on bark is intriguing because the habitat is shared with wood-dwelling mushrooms and physical interaction may be one way the psilocybin BGC could be transferred horizontally. However, the true vector of these HGTs is unknown.

Tempo, Mode, and Timing of the Evolution of the Psilocybin BGC. Previous studies have shown that the psilocybin BGC has been transferred horizontally between several genera of mushrooms within the order *Agaricales* (24, 25). Our analysis combined these data with a much greater representation of *Psilocybe*, recovering the PsiD genes in *Gymnopilus* and *Pluteus* outside of those in *Psilocybe*. In contrast, the copies in *Pholiotina* and *Panaeolus* are nested within the *Psilocybe* PsiD genes. This topology is consistent with ancient divergence between the *Psilocybe* and *Gymnopilus*/*Pluteus* psilocybin BGCs and indicates more recent HGT events between *Psilocybe* and both *Panaeolus* and *Pholiotina*. *Panaeolus cyanescens* appears to have a HGT event with the ancestor of *Psilocybe cubensis*/*subcubensis*. However, the LSU tree indicates that *Pa. subalteatus* is relatively older than *Pa. cyanescens*, and therefore the possibility remains that an earlier HGT event occurred between *Panaeolus* and *Psilocybe*. Interestingly, *Pholiotina smithii* appears to have an HGT event with an ancestor of Clade I, which was recovered with the highest likelihood of a dung ecology in our ancestral state reconstruction. *Pholiotina smithii* and its potentially conspecific relative *Ph. cyanopus* both have terrestrial ecologies in water-saturated and *Sphagnum* moss-dominated soils and grasslands, respectively. However, critical taxa are still missing from the *Psilocybe* phylogeny, such as the *Sphagnum*-associated and non-psilocybin-producing *P. fuscofulva* that has previously been shown to occupy an early-diverging position (45), which may substantially alter the ancestral state reconstructions.

HGT seems to be the most likely explanation for the polyphyletic distribution of the psilocybin BGC. Topological constraint tests of the PsiD phylogeny was performed, and results rejected the alternative hypothesis that recovered psilocybin-producing *Panaeolus* and *Pholiotina* outside of *Psilocybe*, consistent with the hypothesis that the gene cluster was acquired by these two genera

through HGT (25) (*SI Appendix*, Table S4). Additionally, our phylogenetic analyses are consistent with these prior reports and show that the psilocybin BGC has been acquired (likely by HGT) in mushrooms with increasing frequency over the past ~67 mya. In contrast, our molecular dating results provide evidence that the psilocybin BGC has been present in *Psilocybe* between ~56 (MRCA of the genus *Psilocybe*) and ~67 mya (MRCA of *Psilocybe* and *Panaeolus*) (Fig. 3, *Right*). While our LSU dataset presented a more recent divergence estimate for the MRCA of *Psilocybe,* we only included sequences from genera containing psilocybin-producing species so these estimates are likely to be unreliable due to missing taxa. In comparison, divergence dating of our phylogenomic dataset placed the MRCA of all of *Psilocybe* at ~57 mya and the MRCA of *Psilocybe* and *Agrocybe* at ~67 mya (*SI Appendix*).

Our molecular dating analyses relied entirely on secondary calibrations, which are vulnerable to inaccuracies (46). Although these secondary calibrations were derived from studies that used fossil calibrations and we applied uniform rather than normal prior distributions, our absolute dates should still be considered tentative estimates until primary calibrations are available or corroborating evidence is provided. Although a handful of fossil *Agaricales* exist, the closest fossils to *Psilocybe* are *Nidulariaceae*, estimated to be between 45 and 90 mya, but this family is still very distantly related to *Psilocybe* (38, 47). An expanded dataset to enable a single calibration point would be compromised by additional phylogenetic uncertainty. Moreover, many of the available fossils cannot be placed phylogenetically with high confidence due to the dearth of reliable morphological characters. However, regardless of the absolute timing, the presence of the gene cluster in all *Psilocybe* s.s. specimens from this study suggests that the psilocybin BGC is primarily inherited vertically within the genus, although some patterns suggest that this may not be the only mechanism.

The evolution and organization of the psilocybin BGC in *Psilocybe* exhibit some patterns that are consistent with multiple gains or losses. Two different gene orders within the BGC correlate with the earliest divergence within *Psilocybe* (Fig. 2, *Left*), indicating an ancient reconstruction of genes within the genus. Interestingly, the difference in gene order is consistent with a circular transmission model (48), in which the core cluster genes undergo HGT via a circularized intermediate, which linearizes upon insertion into a new genome, proposed for *Pluteus salicinus* in Awan et al. (24). This finding also indicates that transcriptional regulation of the genes may vary among taxa, resulting in taxon-specific metabolic profiles (49, 50). Due to a high number of discontiguous assemblies in our dataset, future studies should place considerable effort on obtaining highly contiguous genomes from modern collections to better refine the psilocybin BGC within *Psilocybe*.

Duplication of PsiH. Upon deeper investigation of PsiH, we found that it had considerably more sequence variation than any of the other core genes and has undergone multiple duplications or multiple losses (Fig. 2 and *SI Appendix*, Table S3). When we included second-best hit identifications to the PsiH phylogeny, we found that the splitting of clade II became less severe, suggesting multiple paralogs are present among many species of *Psilocybe*. PsiH encodes an indole-4-monooxygenase that catalyzes the oxidation of tryptamine at the 4-carbon position of the indole ring (15), a feature that is critical to the pharmacological properties of psilocybin/psilocin and that is both rare in nature and difficult to achieve with traditional synthetic chemistry. This innovation in the psilocybin BGC could be considered the most important to the functioning of the pathway due to its specific activity and is critical for in vivo synthesis of psilocybin in heterologous systems (51, 52). Thus, our study provides additional PsiH sequences that may be useful for optimizing production of psilocybin or other analogs using heterologous expression.

Ecological Role of Psilocybin. Despite its prominence in the scientific and public imagination, experimental evidence for the ecological role of psilocybin is largely lacking and speculation reigns supreme, as thoroughly investigated and reviewed in Meyer and Slot (2023) (53). Psilocybin is a prodrug that is rapidly converted to the dephosphorylated psilocin, which mimics serotonin and binds tightly to serotonin receptors, especially 5-HT_{2A}, a pharmacological action common to psychedelics (54). Serotonin receptors are also found in high concentration in the human gastrointestinal tract, where serotonin signaling is involved in a wide variety of functions, including pain and vomiting (55–57). High-affinity binding to these receptors in mammals, and homologs in distantly related organisms such as insects and arachnids, produces unnatural and altered behaviors (58–61). This disorientation may be a direct deterrent or could render the subject more vulnerable to predation (or, alternatively, may be a reward). However, in humans, the onset of symptoms is delayed by 30 min or more, effectively decoupling the effects from their source. Because of the potentially large effect of psilocybin on GI processes through interactions with serotonin receptors in the gut, it is also possible that psilocybin functions as an emetic or laxative to promote the dispersal of spores before they are rendered inviable by digestion. In fact, nausea is commonly reported in human clinical trials (62). However, other than humans, there are few documented cases of vertebrates consuming psilocybin-containing mushrooms (consisting entirely of domesticated dogs) (63). Many *Psilocybe* mushrooms are uncommon or scarce, and it is difficult to imagine how animals could learn to recognize them with infrequent encounters and delayed pharmacological activity, limiting the selective potential of psilocybin as a psychoactive defense.

Fungal–insect interactions are ancient and widespread and provide a more logical hypothesis for development of psilocybin as a chemical defense in mushrooms (25, 64, 65). To date, this has been the most commonly asserted hypothesis for the ecological role of psilocybin, but empirical studies are still lacking. Furthermore, anecdotes and personal observations confirm that psilocybin-containing mushrooms regularly have living insect larvae in them and they can be reared to adults (24). While not substantive, these anecdotes and initial studies indicate that psilocybin may be ineffective against insects or that some insects may have evolved detoxifying capabilities in response. Moreover, studies demonstrating that psilocybin alters behavior are absent in many non-model insects.

An alternative hypothesis is that psilocybin functions indirectly in an inducible chemical defense system. Lenz et al. (64) elucidated the chemical basis of the blue pigment that forms when psilocybin-containing mushrooms are damaged as oligo/polymers of psilocin. The conversion of psilocybin to psilocin and the linking of them into chains is enzymatically controlled. Lenz et al. (64, 65) pointed out that the psilocin oligo/polymers have chemical properties similar to plant flavonoids and polyphenolic tannins, which produce reactive oxygen molecules that can damage gut tissue. They proposed the "polymer hypothesis," where the psilocin oligo/polymers may be an inducible defense against fungivory and psilocybin is simply the artillery kept in reserve for the true chemical weaponry (64, 65). Intriguingly, the formation of the blue psilocin oligo/polymers is invariably connected to psilocybin biosynthesis throughout the multiple independent

inheritances (24, 25) and convergent evolution (24). The maintenance of the enzymatic capacity to induce psilocybin conversion lends further support to the hypothesis that it is the blue oligo/polymer that has an ecological function rather than the possibly accidental pharmacological effects of psilocybin itself.

Materials and Methods

DNA Extraction and Genomic Sequencing. Hymenophore fragments (5 to 15 mg) from dried fungarium samples, derived from a large collection of institutional loans made to the Natural History Museum of Utah (UMNH) (11) were homogenized by placing them in 2.0 mL screw-cap tubes containing a single 3.0-mm and 8 × 1.5-mm stainless steel beads and shaking them in a BeadBug™ microtube homogenizer (Sigma-Aldrich, #Z763713) for 120 s at a speed setting of 3,500 rpm. For samples collected after 1950, DNA extraction was performed with Monarch® Genomic DNA Purification Kit (NEB, #T3010S) following the manufacturer's protocol for Tissue Lysis with a 1 h incubation at 56 °C except with double the volume of lysis buffer and increasing the amount of wash buffer to 550 µL during each of the wash steps. For samples collected before 1950, including many of the type specimens (see *SI Appendix*, Table S1 for holding institution and collection information), DNA extraction was performed using a phenol-chloroform DNA extraction protocol. In short, after physical homogenization, lysis was performed as above, after which total lysate was placed in Phase Lock Gel™ Light tubes (QuantaBio, #2302820) along with an equal volume of OmniPur® Phenol:Chloroform:Isoamyl Alcohol (25:24:1, TE-saturated, pH 8.0) solution (MilliporeSigma, Calibiochem #D05686) and then mixed by gentle inversion for 15 min using a fixed speed tube rotator. After mixing, tubes were centrifuged at maximum speed (14,000×*g*) for 10 min; then, the aqueous (top) layer was transferred to a new phase-lock gel tube and the process repeated. DNA precipitation of the aqueous phase was performed by adding 5 M NaCl to a final concentration of 0.3 M and two volumes of room temperature absolute ethanol, inverting the tubes 20× for thorough mixing followed by an overnight incubation at −20 °C. The next day, DNA was pelleted by centrifugation at 14,000×*g* for 5 min. The DNA pellet was washed twice with freshly prepared, ice-cold 70% ethanol, air-dried for 15 min at room temperature, and then resuspended in 150 µL of Elution Buffer from the Monarch® Genomic DNA kit. DNAs were submitted to the High Throughput Genomics Core at the University of Utah, where sequencing libraries were prepared using the Nextera™ DNA Flex Library Prep (Illumina®, #20018704) and sequenced on a full lane of Illumina® NovaSeq 6000 PE 2 × 150 bp using an S4 flow cell.

Sequence Processing and Genome Assembly. Sequencing run statistics and quality metric were visualized for each sample using FastQC version 0.11.9 and then compared to each other using MultiQC version 1.10 (66). Library complexity was estimated using the "EstimateLibraryComplexity" function of the Picard toolkit (http://broadinstitute.github.io/picard/). Raw sequencing reads were trimmed and quality filtered using fastP version 0.20.1 (67) and then assembled using the paired-end assembly in SPAdes version 3.15.2 (68) with kmer values alternating every other digit between 21 and 127, inclusive. Genome assembly stats were quantified using a custom Perl script (https://github.com/hobrien/Perl/blob/master/ContigStats.pl).

Homolog Extraction and Phylogenetic Analysis. Single-copy gene families were identified from the *Psilocybe serbica* genome (Psiser1) Markov Cluster (MCL) profile (clustering.2497, https://mycocosm.jgi.doe.gov/clm/run/Psiser1-comparative-qc.2497;SvdlKh?organism=Psiser1) generated by the Joint Genome Institute's (JGI) Mycocosm genome portal (69, 70). This profile included two species of *Psilocybe* (*P. cubensis* (Earle) Singer and *P. serbica*) (15) and six closely related taxonomic outgroups: *Agrocybe pediades* (Fr.) Fayod (Agrped1) (39), *Galerina marginata* (Batsch) Kühner (Galma1) (71), *Gymnopilus chrysopellus* (Berk. & M.A. Curtis) Murrill (Gymch1) (39), *G. junonius* (Fr.) P.D. Orton (Gymjun1) (39), *Hebeloma cylindrosporum* Romagn. (Hebcy2) (72), and *Pholiota alnicola* (Fr.) Singer [=*Flammula alnicola* (Fr.) P. Kumm.)] (Phoaln1) (39). Amino acid sequences of the resulting 2,983 genes in the cluster from Galma1:v1 (*Galerina marginata*) (71) were used as queries for homolog identification in the new assemblies using the "protein2genome" model in exonerate version 2.4.0 (73). The protein2genome model allows for amino acid sequences to be aligned to a genome allowing introns, frameshifts, and exon phase changes in the alignment to better identify orthologous genes, even when distantly related. The output-specific flag "--ryo "%tcs\n"" was also used to extract the sequence information that occurs in the target genome coding sequence of the protein2genome alignment, which was used for further downstream phylogenetic analysis. Nucleotide sequence output from exonerate for each amino acid query was combined and aligned using the multiple sequence alignment program MAFFT version 7.475 (74) with the parameters --maxiterate 1000 --localpair --reorder. Concatenation and multiple sequence alignment summary statistics were performed using the package AMAS (75). Individual gene trees were estimated with IQ-TREE multicore version 2.2.0.3 (76) using ModelFinder (77) and 1,000 ultrafast bootstrap replicates optimized using the --bnni flag (78). A summary coalescent tree was constructed from the individual gene trees using ASTRAL-III (79) after removing branches with low support (BS < 10%). A phylogenomic tree was also constructed from a concatenated supermatrix of all genes using a partitioned analysis in IQ-TREE allowing model selection and model parameter estimation for each gene partition separately with branch lengths shared among all partitions (option -p), and branch supports estimated as above.

Divergence Dating. The fast-dating method of the relative rate framework (RRF), implemented in RelTime and incorporated into the MEGA 11 software package (80–82), was used to estimate divergence times using the ML topology and branch lengths estimated from the concatenated supermatrix with *Psilocybe* s.s. as the ingroup and six selected outgroup taxa (*SI Appendix*, Fig. S1). We chose this method as it has been shown to have comparable accuracy to Bayesian-based approaches but requires far less computational resources (83). However, with 2,983 loci, the computational burden was excessive even with RelTime. Therefore, to further reduce computational burden, we selected a subset of 100 loci from the 2,983 genes whose gene trees were the most clock-like (had the least amount of root-to-tip variation) and had maximal average bipartition support using the package SortaDate (84) to use in RelTime. To calibrate the divergence time estimations, the node representing the most recent common ancestor (MRCA) of *Psilocybe* plus *Agrocybe pediades*, *Galerina marginata*, and *Gymnopilus* spp. [=*Strophariaceae* sensu Varga et al. (38) and *Hymenogastraceae* sensu Ruiz-Dueñas et al. (39)] was constrained using a uniform prior with a minimum of 57 mya [well-supported core shift stem age of *Strophariaceae* s.s.; Varga et al. (38)] and maximum of 71 mya [stem age of the Hymenogastraceae; Ruiz-Dueñas et al. (39)], and fixing the stem age of *Gymnopilus* to 54 mya [Varga et al. (38)]. The number of lineages-through-time (LTT) was estimated with the "ltt" function in the R package ape (85) using log-transformed *y*-values to account for progressively fewer extinction events toward the present.

Incorporating Publicly Available Sequences. Four traditional phylogenetic loci for *Fungi* (ITS, Ef1a, RPB1, and RPB2) were bioinformatically extracted from the genome assemblies using PathRacer (86). PathRacer uses hidden Markov models (HMMs) to query de Bruijn assembly graphs for compatible paths, independent of assembled contiguous sequences, minimizing the limitations of discontiguous assemblies for sequence mining. HMMs were built using nucleotide sequences from 10,859 complete ITS sequences obtained from the NCBI RefSeq Targeted Loci Project (87), and 487 partial EF1a exons, 639 partial RPB1 exons, and 937 partial RPB2 exons generated by AFTOL (88) and downloaded from GenBank, and aligned automatically with the L-INS-i algorithm in MAFFT version 7.475 (74). HMM profiles for each gene were generated with hmmer version 3.1b2 (hmmer.org) using the multiple sequence alignments as inputs. ITS sequences were manually trimmed from edge sequence outputs. Sequences of EF1a, RPB1, and RPB2 were extracted from edge sequence outputs with exonerate using the flag -protein2genome using query protein sequences from *Psilocybe cyanescens* Wakef. in GenBank (GenBank accessions: Ef1a=ADI71893.1; RPB1=AHB18799.1; RPB2=AHH34099.1). All *Psilocybe* sequences corresponding to the same loci (ITS, EF1a, RPB1, and RPB2) were retrieved from NCBI as well as all *Psilocybe* species hypotheses (SH) ITS sequences from the curated fungal database UNITE (89). Each dataset from NCBI was checked for overlap of different genes for a single vouchered specimen using fungarium accession numbers or collections IDs in the GenBank records. The loci extracted from the genomes generated in this study were combined with the publicly available data in single locus matrices and then automatically aligned with the L-INS-i algorithm in MAFFT. Phylogenetic trees for each gene as well as a concatenated supermatrix of the four traditional phylogenetic loci were constructed using IQ-TREE with the same parameters as above, including gene partitions in the concatenated matrix to allow for separate models and model parameters to be estimated per gene,

and with the addition of a backbone constraint using the rooted phylogenomic topology implemented with the -g flag.

Identification of Psilocybin BGC Genes in *Psilocybe*. We used gene prediction and reciprocal-best BLAST (RBB) to identify homologs of gene from the psilocybin BGC in our genome assemblies. Due to the diploid nature of our genomes, we first used the software package Redundans version 0.14a (90) to phase our assemblies before gene prediction. Psilocybin gene cluster detection was performed using the Augustus version 3.4.0 gene prediction software (91) with the flags –singlestrand=true to predict genes independently on each strand with the coprinus_cinereus training set. Following gene prediction, the most likely psilocybin BGC for each species was chosen as follows: Using the protein sequences for PsiD (tryptophan decarboxylase), PsiK (kinase), PsiM (methyltransferase), and PsiH (P450) based on the publicly available chromosomal level assembly for *P. cubensis* (92), we used BLASTP with default parameters to search for homologs in the predicted translated proteins for each species. The top three hits for each gene were then used together to find putative clusters by examining the gene numbers assigned by augustus. Putative "clusters" were identified as any subset of the 21 genes where the predicted gene numbers of any gene within the subset was at most two genes away from one other gene in the subset. This set of computationally generated, putative psilocybin BGCs was then manually curated by querying the top three hits against the Psi gene sequences from the chromosomal assembly of *P. cubensis* using BLASTn to measure their similarities. The largest subset with high similarities to the Psi genes was chosen as the cluster candidate for each *Psilocybe* species (Fig. 2). To corroborate our gene predictions, we utilized exonerate with the same Psi protein queries. Identifications were compared to gene prediction output to determine the order and orientation of each gene in the cluster based on the strand position (+/-) of the start codon for each gene (Fig. 2). Individual gene multiple sequence alignments and maximum likelihood trees were estimated for each psi gene using MAFFT and IQ-TREE as above.

Global PsiD Phylogenetic Analysis, Topological Constraint Testing, and Ancestral State Reconstruction. PsiD nucleotide sequences extracted from all primary psilocybin BGC-containing mushrooms with exonerate were transcribed utilizing codon-aware multiple sequence alignment through HYPHY version 2.5.36 (93) following the tutorial outlined at https://github.com/veg/hyphy-analyses/blob/master/codon-msa/README.md. Extracted PsiD amino acid sequences were combined with the PsiD amino acid sequences published in Reynolds et al. (25), undergoing multiple sequence alignment and phylogenetic analysis under the same parameters used for individual gene trees. Ecological lifestyle was determined from original species descriptions and monographs when available, or directly from collection notes (*SI Appendix*, Table S1).

To test the hypothesis that psilocybin-producing *Panaeolus* (Fr.) Quél. and *Pholiotina* Fayod PsiD are derived within *Psilocybe* PsiD, consistent with HGT, topological constraint testing was performed by comparing the best ML tree constrained to recover a monophyletic *Psilocybe* in IQ-TREE version 1.6.12 with the unconstrained PsiD tree using bootstrap proportion (BP), weighted Kishino–Hasegawa test (94), weighted Shimodaira–Hasegawa test (95), expected likelihood weights (96) with 1,000 RELL replicates, and the approximately unbiased (AU) test (97). An unrooted topological constraint tree was rendered in Mesquite version 3.2 (98).

Ancestral state reconstruction was performed on our concatenated supermatrix phylogenetic tree using RASP 4 (4.3 build 20220517 x64) (99). Each sample was coded for their respective ecological niches (soil, wood, dung, and soil with wood debris) and run under default settings using the MCMC Bayesian option of the Multistate Reconstruction in BayesTraits model (100) (*SI Appendix*). MCMC output was analyzed using Tracer version 1.7.2 (101), which displayed a unimodal distribution supporting convergence with an effective samples size (ESS) of 450 (*SI Appendix*).

Tempo, Mode, and Timing of the Primary Psilocybin BGC. In order to assess the relative timing of psilocybin biosynthesis across mushrooms, a dataset was constructed of all publicly available sequences (194 individuals across 147 species) of the ribosomal large subunit DNA region (28S; downloaded from NCBI on 14 August 2022) for all mushroom genera with species containing the primary psilocybin BGC: *Conocybe* Fayod /*Pholiotina*, *Gymnopilus*, *Panaeolus* Fr., *Pluteus,* and *Psilocybe*. A sequence of *Calocybe gambosa* (Fr.) Donk was used as an outgroup. Due to the poor overlap between taxa for other gene regions, the 28S region had the best species representation that could be aligned across all genera. Multiple sequence alignment was performed using the L-INS-i algorithm in MAFFT. Phylogenetic analysis was performed under maximum likelihood using IQ-TREE with automatic model selection and up to 1,000 nonparametric rapid bootstraps. Divergence dating of the LSU gene tree was performed with RelTime in the same manner as above but with fixed node ages for *Gymnopilus* p.p. (54 mya), *Panaeolus* (60 mya), and *Conocybe* (45 mya) based on Varga et al. (38).

Data, Materials, and Software Availability. Raw short-read sequences for this project have been deposited in the Sequence Read Archive (SRA) and assigned the bioproject number PRJNA904752 and SRA and Biosample accession numbers are reported in *SI Appendix*, Table S1. Raw tree files, assemblies, gene prediction files, multiple sequence alignments, and *Psilocybe* constraint tree are available through Dryad (https://datadryad.org/stash/landing/show?id=doi%3A10.5061%2Fdryad.tmpg4f52s) (102). Any code or specific script requests should be sent to the corresponding author.

ACKNOWLEDGMENTS. We acknowledge the Natural History Museum of Utah for its commitment to collaborative Science and the Genomics Core Facility, a part of the Health Sciences Cores at The University of Utah, for their input and high-quality work. Additionally, we acknowledge the numerous institutions that provided specimens for destructive sampling, many of which were rare and irreplaceable. Further, we wish to recognize the dedicated and hard work performed by Isabelle Galland and Talia A. Backman in their help processing many of these samples for DNA sequencing. Further, we wish to thank David Scott Flocken for his insight and thought-provoking conversations on the work generated here. Additionally, we would like to thank Jan Borovička and Oscar Castro-Jauregui for providing high-quality images and graciously allowing us to use them for publication. We would also like to thank Paul Stamets who provided images and feedback on this publication, and Fungi Perfecti LLC who provided funding which helped facilitate this work. Additionally, we would like to thank Dr. Jason Slot for providing data from previous publications as well as intriguing conversions about Psilocybin evolution. V.R.-C. and L.G.-D. would like to thank the University of Guadalajara and CONAHCYT for their support of their research. This work was supported by a grant from NSF (DEB #2114785) and partially from a generous donation to the NHMU from Fungi Perfecti LLC.

Author affiliations: [a]School of Biological Sciences, University of Utah, Salt Lake City, UT 84112; [b]Natural History Museum of Utah, Collections and Research, University of Utah, Salt Lake City, UT 84108; [c]Consejo Nacional de Humanidades, Ciencias y Tecnologías (CONAHCYT), Departamento de Botánica y Zoología, Universidad de Guadalajara, Zapopan 45147, Mexico; [d]Genomics Innovation Unit, Guy's and St.Thomas' NHS Foundation Trust, St Thomas' Hospital, London SE1 7EH, United Kingdom; [e]Fungi Foundation, Brooklyn, NY 11216; and [f]Departamento de Botánica y Zoología, Universidad de Guadalajara, Zapopan 45147, Mexico

1. R. L. Carhart-Harris *et al.*, The entropic brain: A theory of conscious states informed by neuroimaging research with psychedelic drugs. *Front. Hum. Neurosci.* **8**, 20 (2014).
2. M. W. Johnson, R. R. Griffiths, Potential therapeutic effects of Psilocybin. *Neurotherapeutics* **14**, 734–740 (2017).
3. M. W. Johnson, P. S. Hendricks, F. S. Barrett, R. R. Griffiths, Classic psychedelics: An integrative review of epidemiology, therapeutics, mystical experience, and brain network function. *Pharmacol. Therap.* **197**, 83–102 (2019).
4. E. Fries, Observationes Mycologicae (Havniae: Sumptibus G. Bonnieri, 2021), pp. 1815–1818.
5. R. Heim, R. G. Wasson, *Les Champignons Hallucinogènes du Mexique: Ètudes Ethnologiques, Taxinomiques, Biologiques, Physiologiques et Chimiques* (Museum National d'Histoire Naturelle, 1959).
6. G. Guzmán Huerta, *Nueva localidad de importancia etnomicológica de los hongos neurotrópicos mexicanos* (Necaxa, Puebla) *Ciencia* (México) **20**, 85–88 (1960).
7. N. Echevarria, B. Arochi, M. Sabina, A. Henestrosa, A. Estrada, *María Sabina: Mujer Espíritu [Woman Spirit]* (CONACULTA–IMCINE, 2006).
8. G. Guzmán, Hallucinogenic mushrooms in Mexico: An overview. *Econ. Bot.* **62**, 404–412 (2008).
9. J. Kristinsson, Occurrence and use of hallucinogenic mushrooms containing psilocybin alkaloids (Nordic Council of Ministers, 2008).
10. V. Ramírez-Cruz *et al.*, Phylogenetic inference and trait evolution of the psychedelic mushroom genus *Psilocybe* sensu lato (Agaricales). *Botany* **91**, 573–591 (2013).
11. A. J. Bradshaw *et al.*, DNA authentication and chemical analysis of *Psilocybe* mushrooms reveal widespread misdeterminations in Fungaria and inconsistencies in metabolites. *Appl. Environ. Microbiol.* **88**, e01498-22 (2022).
12. O. S. Castro Jauregui, V. Ramírez-Cruz, A. J. Bradshaw, A. Cortés-Pérez, L. Guzmán-Dávalos, Los hongos sagrados del género *Psilocybe* en Jalisco. *Nubes y Ciencia* **12**, 14–21 (2022).
13. R. C. Van Court *et al.*, Diversity, biology, and history of psilocybin-containing fungi: Suggestions for research and technological development. *Fungal Biol.* **126**, 308–319 (2022).
14. R. G. Wasson, Seeking the magic mushroom. *Life* **49**, 109–120 (1957).

15. J. Fricke, F. Blei, D. Hoffmeister, Enzymatic synthesis of psilocybin. *Angew. Chem. Int. Ed.* **56**, 12352–12355 (2017).
16. J. C. Slot, E. Gluck-Thaler, Metabolic gene clusters, fungal diversity, and the generation of accessory functions. *Curr. Opin. Genet. Dev.* **58–59**, 17–24 (2019).
17. N. P. Keller, Translating biosynthetic gene clusters into fungal armor and weaponry. *Nat. Chem. Biol.* **11**, 671–677 (2015).
18. N. P. Keller, Fungal secondary metabolism: Regulation, function and drug discovery. *Nat. Rev. Microbiol.* **17**, 167–180 (2019).
19. S. R. Waterman, D. W. Holden, Functions and effectors of the *Salmonella* pathogenicity island 2 type III secretion system. *Cell Microbiol.* **5**, 501–511 (2003).
20. A. E. Osbourn, B. Field, Operons. *Cell. Mol. Life Sci.* **66**, 3755–3775 (2009).
21. D. DellaPenna, S. E. O'Connor, Plant gene clusters and opiates. *Science* **336**, 1648–1649 (2012).
22. B. R. Lichman *et al.*, The evolutionary origins of the cat attractant nepetalactone in catnip. *Sci. Adv.* **6**, eaba0721 (2020).
23. I. Burkhardt, T. De Rond, P.Y.-T. Chen, B. S. Moore, Ancient plant-like terpene biosynthesis in corals. *Nat. Chem. Biol.* **18**, 664–669 (2022).
24. A. R. Awan *et al.*, Convergent evolution of psilocybin biosynthesis by psychedelic mushrooms. bioRxiv [Preprint] (2018). https://doi.org/10.1101/374199 (Accessed 15 November 2023).
25. H. T. Reynolds *et al.*, Horizontal gene cluster transfer increased hallucinogenic mushroom diversity. *Evol. Lett.* **2**, 88–101 (2018).
26. K. McKernan *et al.*, A whole genome atlas of 81 *Psilocybe* genomes as a resource for psilocybin production. *F1000Res* **10**, 961 (2021).
27. S. Dörner *et al.*, Genetic survey of *Psilocybe* natural products. *ChemBioChem* **23**, e202200249 (2022).
28. J. Borovička, M. E. Noordeloos, M. Gryndler, M. Oborník, Molecular phylogeny of *Psilocybe cyanescens* complex in Europe, with reference to the position of the secotioid *Weraroa novae-zelandiae*. *Mycol. Progr.* **10**, 149–155 (2011).
29. C. Andrew, J. Diez, T. Y. James, H. Kauserud, Fungarium specimens: A largely untapped source in global change biology and beyond. *Philos. Trans. R. Soc. B* **374**, 20170392 (2019).
30. K. C. Rowe *et al.*, Museum genomics: Low-cost and high-accuracy genetic data from historical specimens. *Mol. Ecol. Resources* **11**, 1082–1092 (2011).
31. K. Bi *et al.*, Unlocking the vault: Next-generation museum population genomics. *Mol. Ecol.* **22**, 6018–6032 (2013).
32. M. Staats *et al.*, Genomic treasure troves: Complete genome sequencing of herbarium and insect museum specimens. *PLoS ONE* **8**, e69189 (2013).
33. G. Besnard *et al.*, From museums to genomics: Old herbarium specimens shed light on a C3 to C4 transition. *J. Exp. Bot.* **65**, 6711–6721 (2014).
34. H. N. Poinar *et al.*, Molecular coproscopy: Dung and diet of the extinct ground sloth *Nothrotheriops shastensis*. *Science* **281**, 402–406 (1998).
35. A. P. Boast *et al.*, Coprolites reveal ecological interactions lost with the extinction of New Zealand birds. *Proc. Natl. Acad. Sci. U.S.A.* **115**, 1546–1551 (2018).
36. S. M. Latorre *et al.*, Museum phylogenomics of extinct *Oryctes* beetles from the Mascarene Islands. bioRxiv [Preprint] (2021). https://doi.org/10.1101/2020.02.19.954339 (Accessed 15 November 2023).
37. B. T. M. Dentinger *et al.*, Tales from the crypt: Genome mining from Fungarium specimens improves resolution of the mushroom tree of life. *Biol. J. Linn. Soc.* **117**, 11–32 (2016).
38. T. Varga *et al.*, Megaphylogeny resolves global patterns of mushroom evolution. *Nat. Ecol. Evol.* **3**, 668–678 (2019).
39. F. J. Ruiz-Dueñas *et al.*, Genomic analysis enlightens agaricales lifestyle evolution and increasing peroxidase diversity. *Mol. Biol. Evol.* **38**, 1428–1446 (2021).
40. Z. Konkel, K. Scott, J. C. Slot, Draft genome sequence of the termite-associated "cuckoo fungus", *Athelia* (*Fibularhizoctonia*) sp. TMB Strain TB5. *Microbiol. Resour. Announc.* **10**, e01230-20 (2021).
41. K. Matsuura, Distribution of termite egg-mimicking fungi ("termite balls") in *Reticulitermes* spp. (Isoptera: Rhinotermitidae) nests in Japan and the United States. *Appl. Entomol. Zool.* **40**, 53–61 (2005).
42. L. Arvidsson, *Athelia arachnoidea* (Berk.) Jül. and its influence on epiphytic cryptogams in urban areas. *Göteborgs Svampklubbs Årsskrift* **1976**, 4–10 (1975).
43. L. Arvidsson, Svampangrepp på lavar–En orsak till lavöken. *Svensk Botanisk Tidskrift* **72**, 285–292 (1979).
44. G. C. Adams, B. R. Kropp, *Athelia arachnoidea*, the sexual state of *Rhizoctonia carotae*, a pathogen of carrot in cold storage. *Mycologia* **88**, 459–472 (1996).
45. J. Borovička *et al.*, Phylogenetic and chemical studies in the potential psychotropic species complex of *Psilocybe atrobrunnea* with taxonomic and nomenclatural notes. *Persoonia* **34**, 1–9 (2015).
46. J. J. Schenk, Consequences of secondary calibrations on divergence time estimates. *PLoS ONE* **11**, e0148228 (2016).
47. M. Sánchez-García *et al.*, Fruiting body form, not nutritional mode, is the major driver of diversification in mushroom-forming fungi. *Proc. Natl. Acad. Sci. U.S.A.* **117**, 32528–32534 (2020).
48. C. M. Johnson, A. D. Grossman, Integrative and conjugative elements (ICEs): What they do and how they work. *Annu. Rev. Genet.* **49**, 577–601 (2015).
49. D. Hoffmeister, N. P. Keller, Natural products of filamentous fungi: Enzymes, genes, and their regulation. *Nat. Prod. Rep.* **24**, 393–416 (2007).
50. W. Yin, N. P. Keller, Transcriptional regulatory elements in fungal secondary metabolism. *J. Microbiol.* **49**, 329–339 (2011).
51. A. M. Adams *et al.*, In vivo production of psilocybin in *E. coli*. *Metab. Eng.* **56**, 111–119 (2019).
52. N. Milne *et al.*, Metabolic engineering of *Saccharomyces cerevisiae* for the de novo production of psilocybin and related tryptamine derivatives. *Metab. Eng.* **60**, 25–36 (2020).
53. M. Meyer, J. Slot, The evolution and ecology of psilocybin in nature. *Fungal Genet. Biol.* **167**, 103812 (2023).
54. A. M. Araújo, F. Carvalho, M. de L. Bastos, P. Guedes de Pinho, M. Carvalho, The hallucinogenic world of tryptamines: An updated review. *Arch. Toxicol.* **89**, 1151–1173 (2015).
55. J. C. Bornstein, Serotonin in the gut: What does it do? *Front. Neurosci.* **6**, 16 (2012).
56. G. M. Mawe, J. M. Hoffman, Serotonin signalling in the gut–functions, dysfunctions and therapeutic targets. *Nat. Rev. Gastroenterol. Hepatol.* **10**, 473–486 (2013).
57. A. S. French *et al.*, The role of serotonin in feeding and gut contractions in the honeybee. *J. Insect. Physiol.* **61**, 8–15 (2014).
58. A. Christiansen, R. Baum, P. N. Witt, Changes in spider webs brought about by mescaline, psilocybin and an increase in body weight. *J. Pharmacol. Exp. Therap.* **136**, 31–37 (1962).
59. C. D. Nichols, J. Ronesi, W. Pratt, E. Sanders-Bush, Hallucinogens and *Drosophila*: Linking serotonin receptor activation to behavior. *Neuroscience* **115**, 979–984 (2002).
60. T. Passie, J. Seifert, U. Schneider, H. M. Emrich, The pharmacology of psilocybin. *Addict. Biol.* **7**, 357–364 (2002).
61. G. R. Boyce *et al.*, Psychoactive plant- and mushroom-associated alkaloids from two behavior modifying cicada pathogens. *Fungal Ecol.* **41**, 147–164 (2019).
62. R. L. Carhart-Harris *et al.*, Psilocybin with psychological support for treatment-resistant depression: An open-label feasibility study. *Lancet Psychiatry* **3**, 619–627 (2016).
63. M. Beug, M. Shaw, K. Cochran, Thirty plus years of mushroom poisoning: Summary of the approximately 2,000 reports in the NAMA Case Registry. *McIlvainea* **16**, 47–68 (2006).
64. C. Lenz *et al.*, Injury-triggered blueing reactions of *Psilocybe* "magic" mushrooms. *Angew. Chem. Int. Ed.* **59**, 1450–1454 (2020).
65. C. Lenz, S. Dörner, A. Sherwood, D. Hoffmeister, Structure elucidation and spectroscopic analysis of chromophores produced by oxidative psilocin dimerization. *Chem. Eur. J.* **27**, 12166–12171 (2021).
66. P. Ewels, M. Magnusson, S. Lundin, M. Käller, MultiQC: Summarize analysis results for multiple tools and samples in a single report. *Bioinformatics* **32**, 3047–3048 (2016).
67. S. Chen, Y. Zhou, Y. Chen, J. Gu, fastp: An ultra-fast all-in-one FASTQ preprocessor. *Bioinformatics* **34**, i884–i890 (2018).
68. A. Bankevich *et al.*, SPAdes: A new genome assembly algorithm and its applications to single-cell sequencing. *J. Comput. Biol.* **19**, 455–477 (2012).
69. I. V. Grigoriev *et al.*, The genome portal of the Department of Energy Joint Genome Institute. *Nucleic Acids Res.* **40**, D26–D32 (2012).
70. I. V. Grigoriev *et al.*, MycoCosm portal: Gearing up for 1000 fungal genomes. *Nucleic Acids Res.* **42**, D699–D704 (2014).
71. R. Riley *et al.*, Extensive sampling of basidiomycete genomes demonstrates inadequacy of the white-rot/brown-rot paradigm for wood decay fungi. *Proc. Natl. Acad. Sci. U.S.A.* **111**, 9923–9928 (2014).
72. Mycorrhizal Genomics Initiative Consortium *et al.*, Convergent losses of decay mechanisms and rapid turnover of symbiosis genes in mycorrhizal mutualists. *Nat. Genet.* **47**, 410–415 (2015).
73. G. S. C. Slater, E. Birney, Automated generation of heuristics for biological sequence comparison. *BMC Bioinf.* **6**, 31 (2005).
74. K. Katoh, MAFFT: A novel method for rapid multiple sequence alignment based on fast Fourier transform. *Nucleic Acids Res.* **30**, 3059–3066 (2002).
75. M. L. Borowiec, AMAS: A fast tool for alignment manipulation and computing of summary statistics. *PeerJ* **4**, e1660 (2016).
76. L.-T. Nguyen, H. A. Schmidt, A. von Haeseler, B. Q. Minh, IQ-TREE: A fast and effective stochastic algorithm for estimating maximum-likelihood phylogenies. *Mol. Biol. Evol.* **32**, 268–274 (2015).
77. S. Kalyaanamoorthy, B. Q. Minh, T. K. F. Wong, A. von Haeseler, L. S. Jermiin, ModelFinder: Fast model selection for accurate phylogenetic estimates. *Nat. Methods* **14**, 587–589 (2017).
78. D. T. Hoang, O. Chernomor, A. von Haeseler, B. Q. Minh, L. S. Vinh, UFBoot2: Improving the ultrafast bootstrap approximation. *Mol. Biol. Evol.* **35**, 518–522 (2018).
79. C. Zhang, M. Rabiee, E. Sayyari, S. Mirarab, ASTRAL-III: Polynomial time species tree reconstruction from partially resolved gene trees. *BMC Bioinf.* **19**, 153 (2018).
80. F. U. Battistuzzi, Q. Tao, L. Jones, K. Tamura, S. Kumar, RelTime relaxes the strict molecular clock throughout the phylogeny. *Genome Biol. Evol.* **10**, 1631–1636 (2018).
81. Q. Tao, K. Tamura, B. Mello, S. Kumar, Reliable confidence intervals for RelTime estimates of evolutionary divergence times. *Mol. Biol. Evol.* **37**, 280–290 (2020).
82. K. Tamura, G. Stecher, S. Kumar, MEGA11: Molecular evolutionary genetics analysis version 11. *Mol. Biol. Evol.* **38**, 3022–3027 (2021).
83. F. P. Costa, C. G. Schrago, B. Mello, Assessing the relative performance of fast molecular dating methods for phylogenomic data. *BMC Genomics* **23**, 798 (2022).
84. S. A. Smith, J. W. Brown, J. F. Walker, So many genes, so little time: A practical approach to divergence-time estimation in the genomic era. *PLoS ONE* **13**, e0197433 (2018).
85. E. Paradis, J. Claude, K. Strimmer, APE: Analyses of phylogenetics and evolution in R language. *Bioinformatics* **20**, 289–290 (2004).
86. A. Shlemov, A. Korobeynikov, "PathRacer: Racing profile HMM paths on assembly graph" in *Algorithms for Computational Biology, Lecture Notes in Computer Science*, I. Holmes, C. Martín-Vide, M. A. Vega-Rodríguez, Eds. (Springer International Publishing, 2019), pp. 80–94.
87. N. A. O'Leary *et al.*, Reference sequence (RefSeq) database at NCBI: Current status, taxonomic expansion, and functional annotation. *Nucleic Acids Res.* **44**, D733–D745 (2016).
88. F. Lutzoni *et al.*, Assembling the fungal tree of life: Progress, classification, and evolution of subcellular traits. *Am. J. Bot.* **91**, 1446–1480 (2004).
89. K. Abarenkov *et al.*, The UNITE database for molecular identification of fungi–Recent updates and future perspectives. *New Phytol.* **186**, 281–285 (2010).
90. L. P. Pryszcz, T. Gabaldón, Redundans: An assembly pipeline for highly heterozygous genomes. *Nucleic Acids Res.* **44**, e113 (2016).
91. M. Stanke *et al.*, AUGUSTUS: Ab initio prediction of alternative transcripts. *Nucleic Acids Res.* **34**, W435–W439 (2006).
92. K. McKernan *et al.*, A draft reference assembly of the *Psilocybe cubensis* genome. *F1000Res* **10**, 281 (2021).
93. S. L. K. Pond, S. D. W. Frost, S. V. Muse, HyPhy: Hypothesis testing using phylogenies. *Bioinformatics* **21**, 676–679 (2005).
94. H. Kishino, M. Hasegawa, Evaluation of the maximum likelihood estimate of the evolutionary tree topologies from DNA sequence data, and the branching order in hominoidea. *J. Mol. Evol.* **29**, 170–179 (1989).
95. H. Shimodaira, M. Hasegawa, Multiple comparisons of log-likelihoods with applications to phylogenetic inference. *Mol. Biol. Evol.* **16**, 1114–1116 (1999).
96. K. Strimmer, A. Rambaut, Inferring confidence sets of possibly misspecified gene trees. *Proc. R. Soc. Lond. B* **269**, 137–142 (2002).
97. H. Shimodaira, An approximately unbiased test of phylogenetic tree selection. *Syst. Biol.* **51**, 492–508 (2002).
98. W. P. Maddison, D. R. Maddison, Mesquite: A modular system for evolutionary analysis (2019).
99. Y. Yu, C. Blair, X. He, RASP 4: Ancestral state reconstruction tool for multiple genes and characters. *Mol. Biol. Evol.* **37**, 604–606 (2020).
100. A. Meade, M. Pagel, "Ancestral state reconstruction using BayesTraits" in *Environmental Microbial Evolution, Methods in Molecular Biology*, H. Luo, Ed. (Springer, US, 2022), pp. 255–266.
101. A. Rambaut, A. J. Drummond, D. Xie, G. Baele, M. A. Suchard, Posterior summarization in Bayesian phylogenetics using Tracer 1.7. *Syst. Biol.* **67**, 901–904 (2018).
102. A. Bradshaw *et al.*, Phylogenomics of the psychoactive mushroom genus Psilocybe and evolution of the psilocybin biosynthetic gene cluster [Dataset]. Dryad. https://datadryad.org/stash/landing/show?id=doi:10.5061/dryad.tmpg4f52s. Deposited 6 November 2023.